CHEMISTRY OF MATERIALS

pubs.acs.org/cm

Article

Cobalt Tritolylcarboxy Porphyrin-Carbon Black Composite Bifunctional Electrocatalyst for Nitrate and Carbon Dioxide Electroreduction to Ammonia and Formic/Acetic Acid

Published as part of Chemistry of Materials special issue "Bifunctional Electrocatalysts".

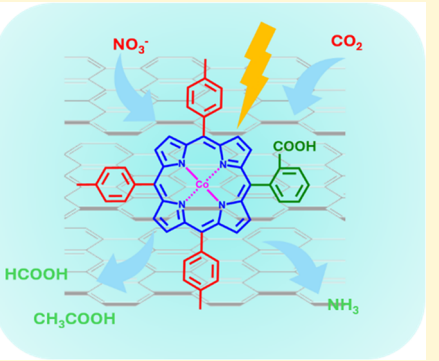
Kamal Dhakal,[§] Alankar Kafle,[§] Swatej Sabbarwal, Dili R. Subedi, Mohammad K. Altafi, Alireza Hajiseyedjavadi, Sayan Maiti, Shengqian Ma, Thomas R. Cundari,* and Francis D'Souza*

Cite This: *Chem. Mater.* 2026, 38, 9791−9801

Read Online

ACCESS | Metrics & More | Article Recommendations | Supporting Information

ABSTRACT: Electrochemical nitrate reduction reaction (NO_3RR) and carbon dioxide reduction reactions (CO_2RR) can serve as environmental remediation tools for pollution control and thus support a circular economy for sustainability. The electrochemical process relies heavily on electrode materials; thus, developing highly active and efficient electrocatalysts for these reactions in a green and cost-effective way is essential. In this study, we examined cobalt porphyrins with different modifications for electrochemical NO_3RR and CO_2RR to independently produce ammonia and acetic acid/formic acid. The carboxylic acid group-substituted cobalt tetrakis(p-tolyl) porphyrin showed a high Faradaic efficiency of 94% for ammonia, 33.8% for CH_3COOH, and 21.1% for HCOOH at various potentials in a neutral pH (∼7) electrolyte. Computational results suggest enhanced binding of key NO_3RR and CO_2RR intermediates to the −COOH group-substituted cobalt porphyrin during electrocatalysis.



1. INTRODUCTION

The growing global population, combined with widespread industrialization, rapid urbanization, and excessive natural resource extraction, has led to a significant increase in waste production and emissions, resulting in severe environmental pollution.[1−5] Among many industrial pollutants, CO_2 and NO_3^- are particularly significant because they originate in large quantities from fuel combustion, agriculture, and manufacturing processes.[6,7] Excess CO_2 in the atmosphere worsens the greenhouse effect, while high levels of NO_3^- in water cause oxygen depletion and eutrophication, harming aquatic ecosystems and threatening drinking water quality, which endangers human livelihoods.[8,9] Thus, effective environmental remediation is vital to protect human health and restore ecosystems. Various strategies for converting CO_2, such as thermochemical, photochemical, biochemical, and electrochemical methods, are currently used.[10,11] Similarly, techniques like biological denitrification, constructed wetlands, ion-exchange, reverse osmosis/nanofiltration, and electrochemical methods are common for removing nitrate ions.[12−17] Among these, electrochemical approaches stand out as a promising solution because they can treat pollutants in mild aqueous conditions at ambient temperatures using renewable electricity. Additionally, the electrochemical conversion of these pollutants via the carbon dioxide reduction reaction (CO_2RR) and nitrate reduction reaction (NO_3RR) not only facilitates environmental remediation but also promotes sustainability by generating economically valuable fuels and chemical feedstocks. Therefore, developing high-performance electrode materials of good stability for electrocatalytic CO_2RR and NO_3RR, which produce high-value chemicals with good selectivity and energy efficiency, is a crucial objective currently.

In this context, numerous studies have aimed to develop highly effective electrocatalysts for the catalytic reduction of CO_2 and NO_3 separately to selectively produce valuable products. A variety of materials, including metal/alloy nanoparticles,[18−20] metal chalcogenides,[21−23] graphitic carbonaceous materials,[24,25] metal−organic frameworks,[26,27] metalloporphyrins,[28,29] metallopthalocyanines,[30,31] *etc.*, have been explored for both reactions. Among these, molecular catalysts attract significant attention over solid-state catalysts because their well-defined structures enable the identification of active sites and facilitate the development of structural models for computational studies, which lead to mechanistic insights.[32]

Received: March 10, 2026
Revised: September 15, 2026
Accepted: September 17, 2026
Published: September 29, 2026



ACS Publications © 2026 American Chemical Society

Downloaded from pubs.acs.org/cmatex/article-pdf/38/19/9791/6870339l/acs.chemmater.6c00705.pdf by UNIV OF NORTH TEXAS user on 21 October 2026

Additionally, the relationship between molecular structure and electrocatalytic activity offers opportunities for rational design and activity optimization of electrocatalysts through fine-tuning their coordination environments.[32−35] Metalloporphyrins, a type of coordination compound featuring a central metal coordinated to a porphyrin ligand, have been extensively studied in electrocatalysis.[36] Their synthetic flexibility enables a systematic exploration of how the attached group to the porphyrin nucleus influences both the electrocatalytic activity and the selectivity of the products.

Jiang et al. studied the role of electron-donating/withdrawing groups, $-OCH_3$ and $-Br$, attached to Cu tetraphenylporphyrin (Cu−THPP) toward CO_2RR.[37] Similarly, Sun et al. demonstrated the alteration in the electrocatalytic NO_2RR activity with the structural modification of the porphyrin molecule by variation of electron-donating/withdrawing groups in iron 4,4′,4″,4‴-(porphyrin-5,10,15,20-tetrayl)tetrakis(*N*,*N*-dimethylaniline) (FeDMA) and iron 4,4′,4″,4‴-(porphyrin-5,10,15,20-tetrayl)tetrakis(*N*,*N*,*N*-trimethylbenzenaminium) (FeTMA), achieving significant enhancement in ammonia yield.[38] Although the fine-tuning of the structure of these materials can provide high selectivity toward the target catalytic reactions, the low intrinsic electrical conductivity of metalloporphyrin complexes limits their electrocatalytic performance. During electrocatalysis, conductive carbon supports can be employed for enhancing charge transport in the electrode−electrolyte interface because of their excellent electrical conductivity. Therefore, the combination of metalloporphyrin with graphitic carbon support was explored as a functional material for electrocatalytic applications. Moreover, the immobilization of metalloporphyrin with graphitic carbonaceous materials such as carbon black (Vulcan carbon), carbon nanotubes, graphene, and others enables noncovalent $\pi-\pi$ stacking interactions between the π-conjugated sidewalls of the CNTs and the aromatic macrocycle of the porphyrin. As a result, the porphyrin molecule binds to graphitic carbonaceous materials, enhancing catalytic activity by promoting optimal utilization of active sites, increasing surface area and porosity, and ultimately improving electron transfer and electrocatalytic performance.[33,36] For example, Maurin et al. explored a Fe porphyrin−CNT composite toward CO_2RR for achieving 90% Faradaic efficiency for CO production.[39] Similarly, Choi et al. employed a Fe porphyrin/graphene hybrid (FePGF) and exhibited 97% Faradaic efficiency for CO production at a low overpotential.[40] Importantly, while much effort has been dedicated to exploring individual CO_2RR or NO_3RR electrocatalysts, the development of a bifunctional electrocatalyst capable of both CO_2RR and NO_3RR remains rare.

Herein, we propose a cobalt tritolyl carboxy porphyrin (CoTTPCOOH) immobilized on carbon black (Vulcan carbon) as a bifunctional electrocatalyst for the CO_2RR and NO_3RR, aiming to produce high-value chemicals such as ammonia, acetic acid, and formic acid as major electrolysis products. As expected, the CoTTPCOOH/VC demonstrated superior performance with a Faradaic efficiency of 94% for ammonia during NO_3RR. It also achieved Faradaic efficiencies of 31% for CH_3COOH and 21% for HCOOH during CO_2RR in a neutral pH (∼7) electrolyte. Computational results indicate that key NO_3RR and CO_2RR intermediates bind to the −COOH group on the cobalt porphyrin, facilitating the electrocatalytic processes.

2. RESULTS AND DISCUSSION

2.1. Synthesis and Characterization of Materials

Figure S1 summarizes the CoTTPCOOH synthesis (see the Experimental Section and characterization spectral details, Figures S2−S6). Tetrakis(p-tolyl) porphyrin $TTPCOOCH_3$ (**1**) was synthesized by refluxing p-tolualdehyde, pyrrole, and *o*-methoxycarbonyl benzaldehyde with propionic acid, following the reported literature.[41] The metalation reaction for complexation of $TTPCOOCH_3$ with cobalt was carried out by reacting compound (**1**) with cobalt acetate in DMF to produce compound (**2**), which was then converted to compound (**3**), namely, cobalt tritolyl carboxy porphyrin (CoTTPCOOH) upon hydrolysis. Various characterization techniques were employed to confirm the successful synthesis of CoTTPCOOH. Primarily, UV−vis spectrometry was employed to analyze the formation of $TTPCOOCH_3$; the presence of one Soret band and four Q-bands in the UV−vis spectra indicated its formation, which was further confirmed by ^{1}H NMR spectroscopy. The ^{1}H NMR spectra showed characteristic peaks at δ = 9.00−8.90 (m, 8H, B-pyrrole); 8.46 (dd, 4H,*J* = 46, 6 Hz, carbomethoxyphenyl-3,4,5,6-proton); 8.17 (d, 6H, *J* = 16 Hz, tolyl-2,6-protons); 7.59(d, 6H, *J* = 8 Hz, tolyl-3,5-protons); 4.17 (s, 3H, methyl easter); 2.75 (s, 9H, methyls); −2.59(s, 2H, pyrrole N−H) recorded with 400 MHz, $CDCl_3$, confirming the molecular structure of $TTPCOOCH_3$ (Figure S2). After complexing compound (**1**) with cobalt and subsequent hydrolysis, ^{1}H NMR spectra exhibited deshielded broad peaks with an equivalent number of respective protons at different chemical shift values (δ, ppm) such as 12.8 (s, 8H; β-pyrrole-H), 9.20 (s, 4H, Ar−H), 8.0−8.5 (m, 8H, Ar−H), 7.52 (s, 3H; Ar−H), 3.3 (s, 9H; methyl) corresponding to CoTTPCOOH (Figure S3) that was further confirmed from the UV−vis spectra showing one Soret band and one Q-bands, consistent with the formation of the Co-porphyrin complex **3** (Figure S4a). Complex **3**, i.e., CoTTPCOOH, was further investigated with Raman and IR spectroscopy. The Raman spectra revealed the characteristic peaks corresponding to Co−N stretching (390 cm^{-1}), pyrrole ring deformation (1350 cm^{-1}), and C=C/C−N stretching (1585 cm^{-1}) along with C=O (1700 cm^{-1}) stretching and C−O stretching (1225 cm^{-1}) corresponding to the −COOH group (Figure S4b).[42] Likewise, the existence of characteristic bands such as C−N stretching (1350 cm^{-1}), pyrrole ring stretching (1500 cm^{-1}), and C−C skeleton vibrations (1450 cm^{-1}) associated with the porphyrin ring, as well as C=O stretching (1710 cm^{-1}) and O−H stretching (2850 cm^{-1}) in IR spectra (Figure S4c) confirmed the formation of CoTTPCOOH.[43,44] Additionally, the presence of a base peak at *m*/*z* 756 in the mass spectrum of CoTTPCOOH (Figure S5) confirmed its molecular structure. As the main aim of this material is to explore its application in electrocatalysis, we also performed electrochemical characterizations using cyclic voltammetry (CV) and differential pulse voltammetry (DPV). As shown in Figure S6, the CoTTPCOOH revealed one reversible and one quasi-reversible oxidation peak at 1.0 and 1.43 V vs Ag/AgCl, respectively, along with one quasireversible reduction peak at −1.1 V vs Ag/AgCl, indicating the potentiality of the material for electron transfer and stability during electrolysis within the suggested potential window. The CoTTPCOOH-immobilized carbon black (Vulcan carbon), i.e., COTTPCOOH/VC, was further characterized via powder X-ray Diffraction (PXRD), Scanning Electron Microscopy (SEM), Energy-Dispersive X-ray Spec-

Downloaded from pubs.acs.org/cmatex/article-pdf/38/19/9791/6870339/1/acs.chemmater.6c00705.pdf by UNIV OF NORTH TEXAS user on 21 October 2026

https://doi.org/10.1021/acs.chemmater.6c00705
Chem. Mater. 2026, 38, 9791−9801

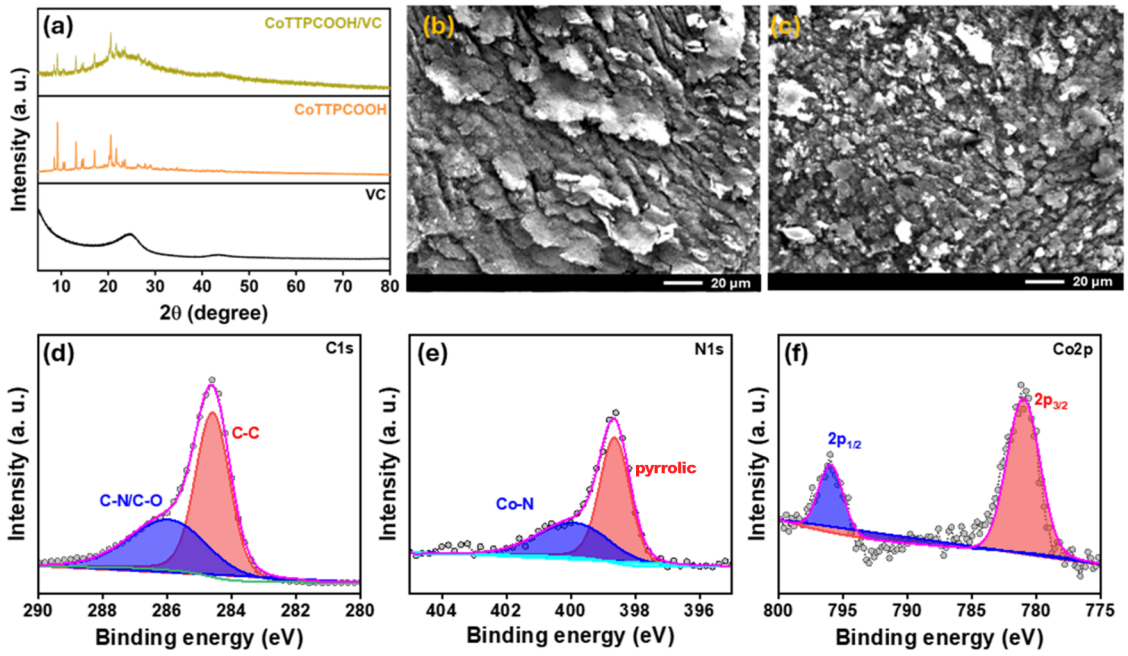


Figure 1. (a) PXRD pattern of VC, CoTTPCOOH and CoTTPCOOH/VC, SEM images of (b) VC, (c) CoTTPCOOH/VC, and deconvoluted XPS spectra of (d) C 1s, (e) N 1s, and (f) Co 2p for CoTTPCOOH/VC.

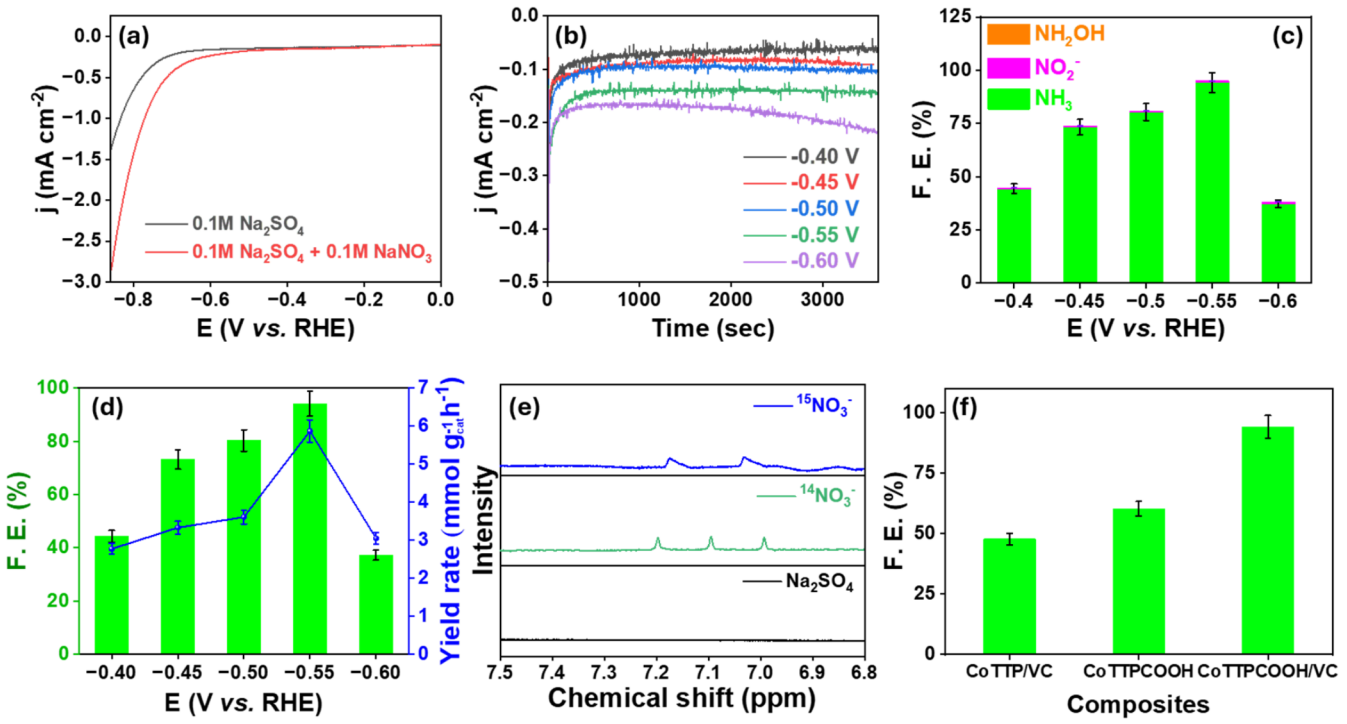


Figure 2. (a) Linear sweep voltammograms in 0.1 M $NaNO_3$ and 0.1 M Na_2SO_4 solution acquired at a scan rate of 10 mV s^{-1}, (b) chronoamperometric curves in 0.1 M $NaNO_3$ + 0.1 M Na_2SO_4 solution at different potentials (c) nitrate reduction faradic efficiency, (d) NH_3 production yield rate and Faradaic efficiency at different applied potentials (e) ^1H NMR spectra for NH_3 produced from different electrolyte samples for isotope labeling experiment for CoTTPCOOH/VC and (f) comparison of Faradaic efficiency for ammonia production catalyzed by various materials.

troscopy (EDS), and X-ray Photoelectron Spectroscopy (XPS) studies. The PXRD patterns of VC, CoTTPCOOH, and COTTPCOOH/VC composites are shown in Figure 1a. The two characteristic diffraction peaks around 2θ values 26° (002) and 43° (100) for VC correspond to graphite character.[45] Similarly, in the case of CoTTPCOOH, a characteristic peak was observed at 2θ values of 29° relevant to metal porphyrins, along with crystalline fingerprint porphyrin peaks.[45−47] The composite materials, COTTPCOOH/VC, exhibited signals of both VC and COTTPCOOH. The retention of the characteristic diffraction peaks with a decrease in the peak intensity after compositing porphyrin with Vulcan carbon confirmed the

https://doi.org/10.1021/acs.chemmater.6c00705
Chem. Mater. 2026, 38, 9791−9801

Downloaded from pubs.acs.org/cmatex/article-pdf/38/19/9791/6870339/1/acs.chemmater.6c00705.pdf by UNIV OF NORTH TEXAS user on 21 October 2026

composite formation, whereas the broad peak in the composite material refers to restored electronic conjugation of the VC carbon framework as well as supports the interaction between VC and CoTTPCOOH.[48−50] The SEM images of VC and CoTTPCOOH/VC are presented in Figure 1b,c. The SEM images revealed that the CoTTPCOOH/VC composite exhibited a faintly more aggregated and roughened morphology, supported by the appearance of particle-like deposits that can be ascribed to COTTPCOOH aggregates anchored onto the surface of Vulcan carbon. Additionally, the observed homogeneous distribution of Co, N, and C throughout the CoTTPCOOH/VC composite in EDS elemental mapping (Figure S7) further supports the uniform dispersion of CoTTPCOOH on the Vulcan carbon, suggesting successful immobilization of the metalloporphyrin with Vulcan carbon. The XPS study was employed to analyze the chemical states of the elements in CoTTPCOOH/VC. The survey spectra of the CoTTPCOOH/VC demonstrated the presence of key elements C, N, O, and Co (Figure S8a). The high-resolution deconvoluted XPS spectra for C 1s exhibited two bands at binding energies of 284.5 and 286.5 eV, corresponding to the C−C and C−O/C−N moieties, respectively (Figure 1c).[51] Similarly, two characteristic bands around 399.0 and 400.5 eV were observed in the deconvoluted N 1s spectrum, assigned to N−C and N−Co, respectively[52] (Figure 1d), whereas the two peaks in the O 1s spectrum were attributed to C═O and C−O moieties[51] (Figure S8b). The deconvoluted Co 2p spectrum demonstrated Co $2p_{1/2}$ and Co $2p_{3/2}$ peaks at 781 and 796 eV, inferring the existence of cobalt in the Co (II) form[51] in CoTTPCOOH (Figure 1e). A comparative analysis of deconvoluted XPS spectra of CoTTPCOOH and CoTTPCOOH/VC (Figures 1d−f and S9) was employed to confirm the interaction of porphyrin molecules, with graphitic carbon support. The observed significant change in binding energy of Co 2p3/2 (∼ +1 eV) and N 1s (∼ +0.3 eV) after composite formation confirmed the interaction of the porphyrin molecules with carbon supports via $\pi-\pi$ stacking.[53,54]

Furthermore, the surface area and pore size distribution of the CoTTPCOOH/VC were studied using the Brunauer−Emmett−Teller (BET) technique. The composite material CoTTPCOOH/VC exhibited a specific surface area of approximately 16 $m^2\ g^{-1}$ and mesoporous porosity (Figure S10), which can enhance mass transport and promote electrolyte diffusion through the porous structure.

2.2. Electrocatalytic NO_3RR Activity

Following the successful characterization of CoTTPCOOH, its potential for electrocatalytic nitrate reduction was evaluated. An H-type cell with two compartments separated by a Nafion membrane was used for electrochemical studies. The catalyst slurry was prepared by dispersing a uniform mixture of CoTTPCOOH and VC (7:3) in isopropyl alcohol, then water. A similar method was used for preparing other control materials. The electrochemical cell featured a catalyst slurry-coated glassy carbon working electrode, with Ag/AgCl (3 M KCl) and Pt-wire electrodes serving as reference and counter electrodes, respectively. Initially, linear sweep voltammograms were recorded in 0.1 M Na_2SO_4 and 0.1 M Na_2SO_4 + 0.1 M $NaNO_3$ electrolytes separately. The CoTTPCOOH/VC showed (Figure 2a) a higher current density in the electrolyte containing nitrate, indicating successful nitrate reduction under applied potential and suggesting the material's promising electrocatalytic activity toward NO_3RR. Detailed performance evaluation involved chronoamperometric electrolysis at various potentials for 1 h (Figure 2b), followed by product analysis. Water-soluble NO_3RR products such as NH_3, NH_2NH_2, NO_2^-, and NH_2OH were spectrophotometrically analyzed using indophenol blue, Watt and Chrisp NEDA coupling, and o-phenanthroline methods, respectively (see details in SI). Calibration curves were generated from solutions of various concentrations to quantify these products (Figure S11). The Faradaic efficiency trends for different NO_3RR products at various potentials estimated from chronoamperometry followed by product quantification via corresponding UV−vis absorbance spectra are summarized in Figures 2c and S12. The CoTTPCOOH/VC achieved a maximum NO_3RR Faradaic efficiency of 95% at −0.55 V vs RHE. A similar trend was observed for ammonia production, with a highest Faradaic efficiency of 94.1% and a production rate of 5.87 mmol $g_{cat}^{-1}\ h^{-1}$ at the same potential (Figure 2d). Since all electrochemical studies were conducted on a laboratory scale and ammonia amounts were small, contamination risks exist, especially since the catalyst contains N-groups in its structure, which could lead to false positives. To verify that the ammonia detected in the catholyte after electrolysis was produced by NO_3RR rather than other sources, an isotope-labeling experiment was performed. Electrolysis was carried out using three electrolyte solutions: 0.1 M Na_2SO_4, 0.1 M Na_2SO_4 + 0.1 M $NaNO_3$, and 0.1 M Na_2SO_4 + 0.1 M $Na^{15}NO_3$, with products analyzed by ^1H NMR spectroscopy. The spectra of products from 0.1 M Na_2SO_4 + 0.1 M $NaNO_3$ showed a triplet with a 52 Hz coupling constant, while a doublet with a 75 Hz coupling constant was observed with 0.1 M Na_2SO_4 + 0.1 M $Na^{15}NO_3^-$ no such signals appeared with Na_2SO_4 alone (Figure 2e). Similarly, to ensure that porphyrin nitrogen was not involved in ammonia formation, we performed another electrolysis study in the absence of nitrate ions using a 3-fold higher catalyst loading on the electrode, and recorded ^1H NMR spectra for product analysis. The absence of any characteristic peak corresponding to ammonia in the ^1H NMR spectrum confirmed the noninvolvement of any type of background contamination. (Figure S13).

These results confirmed that the ammonia detected after electrolysis was exclusively produced during nitrate reduction. Beyond excellent electrocatalytic activity, the electrode's sustained performance and long-term stability are essential indicators. A 12 h chronoamperometry at −0.55 V vs RHE was conducted, followed by postelectrolysis characterization using SEM, EDS, UV−vis, and Raman spectroscopy. The current density over time (Figure S14) remained stable, demonstrating the electrode material's electrochemical stability. Moreover, the characteristic morphological attributes, elemental distribution, and spectral bands in UV−vis and Raman spectra persisted even after long-term electrolysis, further confirming the durability of the material (Figures S15 and S16).

After establishing the promising NO_3RR activity of the CoTTPCOOH/VC, the influence of the conductive carbon support and the functional group attached to the molecule was also examined through a series of control experiments. The NO_3RR performance of CoTTPCOOH and CoTTP/VC was assessed using LSV and chronoamperometry, followed by product analysis. Comparing the LSVs of CoTTPCOOH (Figure S17a), a higher current density in 0.1 M Na_2SO_4 + 0.1 M $NaNO_3$ than in 0.1 M Na_2SO_4 solution was observed, signifying the potential NO_3RR activity of the material. The detailed evaluation of NO_3RR activity by product assessment

Downloaded from pubs.acs.org/cmatex/article-pdf/38/19/9791/6870339/1/acs.chemmater.6c00705.pdf by UNIV OF NORTH TEXAS user on 21 October 2026

https://doi.org/10.1021/acs.chemmater.6c00705
Chem. Mater. 2026, 38, 9791−9801

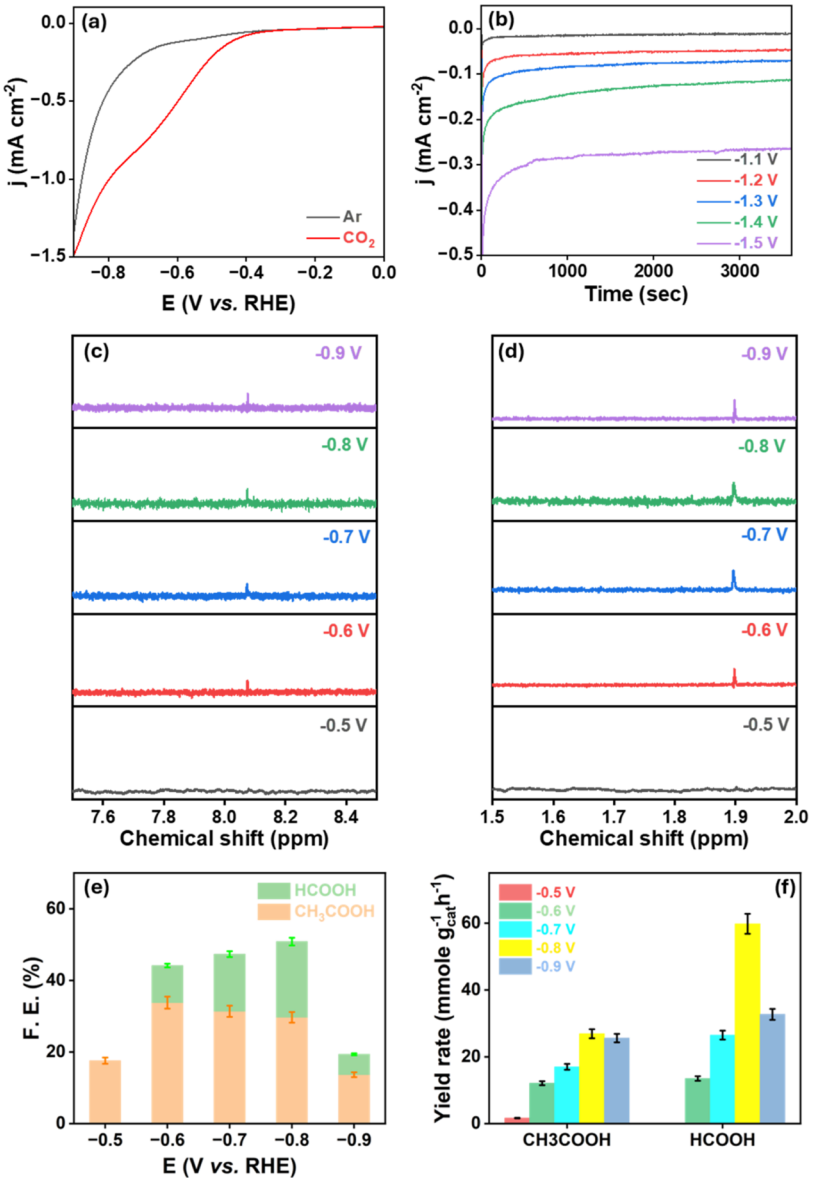


Figure 3. (a) Linear sweep voltammogram in CO_2 and Ar-saturated 0.1 M $KHCO_3$ solutions recorded with a scan rate of 10 mV/s, (b) current density vs time plot recorded during chronoamperometric electrolysis at different potentials. Selected area zoomed ^1H NMR spectra showing characteristic peaks corresponding to (c) HCOOH and (d) CH_3COOH, (e) faradaic efficiency, and (f) yield rate for HCOOH and CH_3COOH during CO_2RR catalyzed by CoTTPCOOH/VC.

revealed the maximum Faradaic efficiency of 60.2% at −0.6 V vs RHE (Figures 2f, S17b−f, and S18). The observed higher Faradaic efficiency of CoTTPCOOH/VC than that of CoTTPCOOH evidenced the role of VC in enhancing electrocatalytic activity. Compositing the porphyrin molecules with Vulcan carbon leads to noncovalent $\pi-\pi$ stacking interactions between VC and the porphyrin molecule, increasing surface area, improving porosity, and optimizing active-site utilization, ultimately enhancing electron transfer and improving electrocatalytic activity.[33] Likewise, the role of the functional group attached to the metalloporphyrin moiety was assessed by comparing the NO_3RR activity of the −COOH group-containing CoTTPCOOH/VC with −COOH group-free CoTTP/VC. Although the LSVs and electrolysis results of CoTTP/VC (Figures 2f, S19a−f, and S20) exhibit the NO_3RR activity with a maximum Faradaic efficiency of 47.7% at −0.55 V vs RHE for ammonia production, but found to be inferior compared to CoTTPCOOH/VC, inferring that the −COOH group can provide better electron transfer leading to enhancement in electrocatalytic activity, which is further analyzed by performing electrochemical impedance spectroscopy (EIS) and electrochemical surface area (ECSA) studies. Since the information about charge transfer resistance (R_{ct}) obtained from EIS can be employed for the evaluation of electrocatalytic activity, a lower R_{ct} indicates faster electron transfer and enhanced electrocatalytic activity.[55,56] Similarly, ECSA insights into the number of active sites of the material, where a higher ECSA implies better catalytic activity.[55,56] The observed lower charge transfer resistance and higher ECSA for CoTTPCOOH/VC 7 ohm and 7.05 cm^2 respectively, than those for CoTTP/VC 14 ohm and 5.77 cm^2 (Figures S21−22 and Tables S1−2), respectively, reveal its superior electrocatalytic activity. These control-experiment results suggest that compositing CoTTPCOOH

https://doi.org/10.1021/acs.chemmater.6c00705
Chem. Mater. 2026, 38, 9791−9801

Downloaded from pubs.acs.org/cmatex/article-pdf/38/19/9791/6870339/1/acs.chemmater.6c00705.pdf by UNIV OF NORTH TEXAS user on 21 October 2026

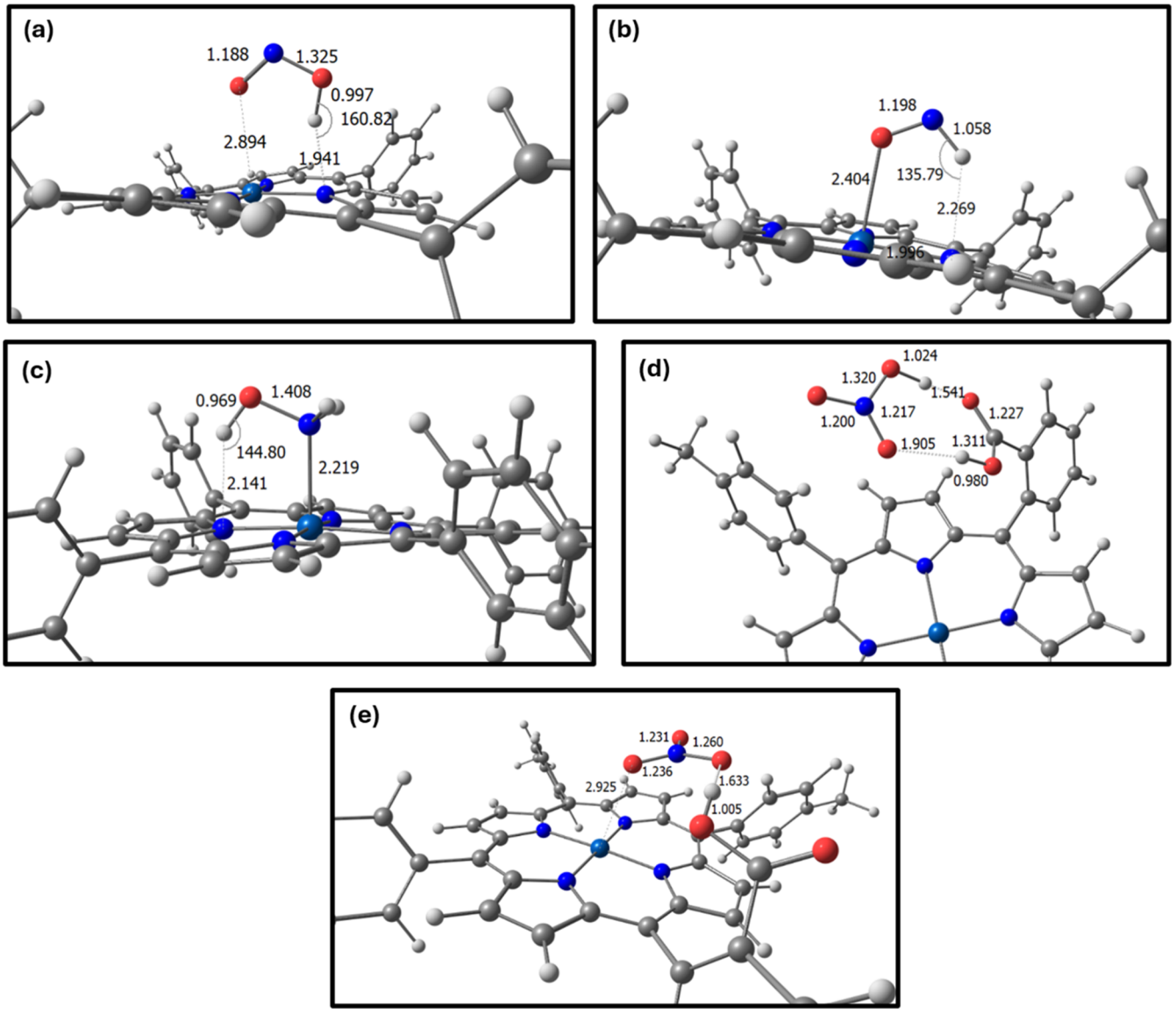


Figure 4. DFT-optimized structure of (a) nitrous acid, (b) nitroxyl, (c) hydroxylamine, (d) nitric acid, and (e) nitrate.

with Vulcan carbon can significantly improve its electrocatalytic performance. Similarly, functionalization of the cobalt tetratolyl porphyrin with a −COOH group leads to better electrocatalytic activity toward NO_3RR.

2.3. Electrocatalytic CO_2RR Activity

Inspired by the effective electrocatalytic activity of CoTTPCOOH toward NO_3RR, the same material is further explored for CO_2RR. A gastight H-type cell filled with 0.1 M $KHCO_3$ solution and separated with a Nafion membrane was employed for CO_2RR evaluation. Before running the electrochemical experiments, the electrolyte was saturated with CO_2 gas. First, CO_2RR activity was analyzed by performing LSVs in Ar and CO_2-saturated electrolytes separately from a potential of 0.0 to −0.9 V vs RHE. Since the higher Faradaic current in the CO_2-saturated electrolyte than that in the Ar-saturated electrolyte in the LSVs mostly signifies the electrocatalytic activity of the material toward CO_2RR. The LSVs of CoTTPCOOH revealed a sharp increase in current density after 0.5 V vs RHE in the CO_2-saturated electrolyte. On the other hand, a similar increment in current density was observed after 0.6 V vs RHE when the electrolyte solution was saturated with Ar-gas. The observed higher current density in the CO_2-saturated electrolyte than in the Ar-saturated electrolyte (Figure 3a) witnessed a successful electroreduction of CO_2 molecules catalyzed by CoTTPCOOH/VC. To assess the detailed CO_2RR activity of the material, a series of chronoamperometric studies was performed at various potentials (Figure 3b), and the water-soluble electrolysis products were examined using ^1H NMR spectroscopy. The ^1H NMR spectra of the electrolyte solution after electrolysis exhibited characteristic peaks around 2.0 and 8.5 ppm corresponding to acetic acid and formic acid, respectively (Figure 3c,d). To analyze the water-soluble CO_2RR products, we generated calibration curves using a series of ^1H NMR spectra of standard solutions of formic acid and acetic acid, with maleic acid as an internal standard (Figures S23 and S24).

The CoTTPCOOH/VC revealed a maximum Faradaic efficiency of around 51% to produce water-soluble HCOOH and CH_3COOH together at −0.8 V vs RHE (Figure 3e). While assessing the selectivity toward particular CO_2RR products, the CoTTPCOOH/VC demonstrated a maximum

https://doi.org/10.1021/acs.chemmater.6c00705
Chem. Mater. 2026, 38, 9791−9801

Downloaded from pubs.acs.org/cmatex/article-pdf/38/19/9791/6870339/1/acs.chemmater.6c00705.pdf by UNIV OF NORTH TEXAS user on 21 October 2026

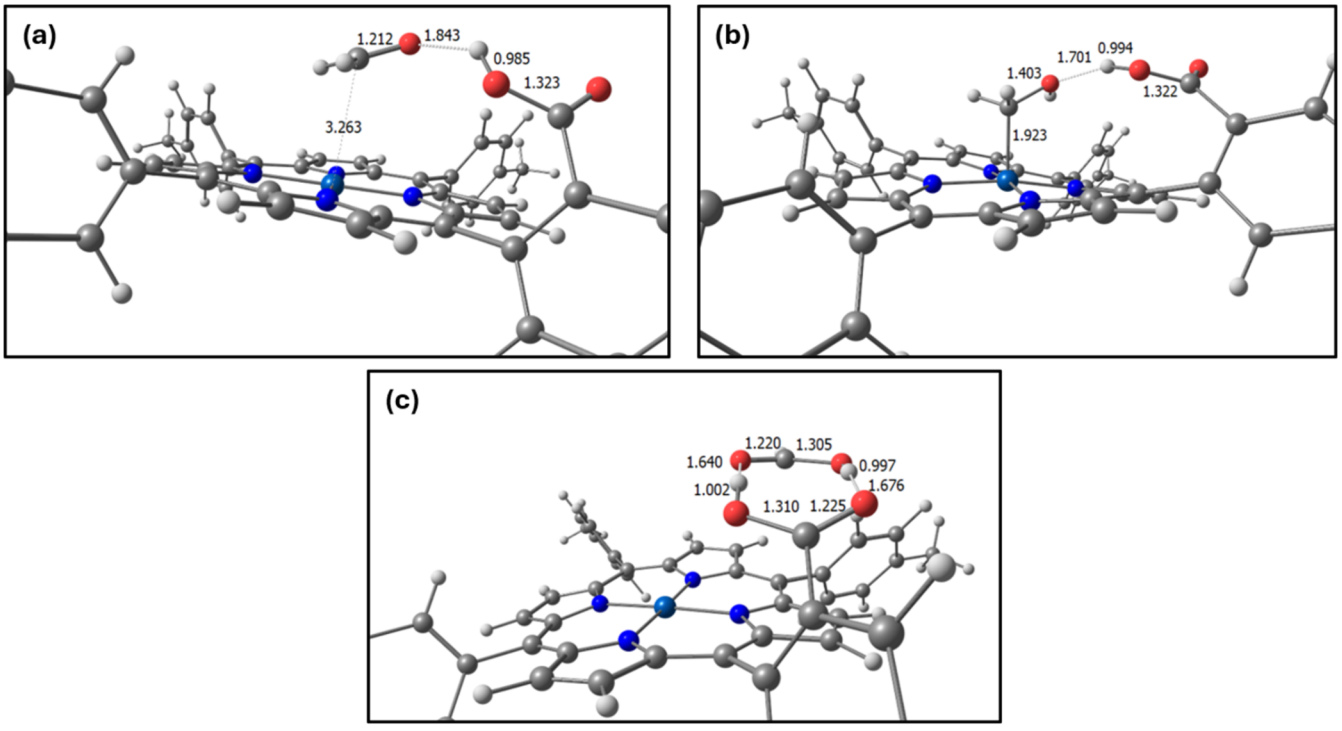


Figure 5. DFT-optimized structure of (a) formaldehyde, (b) *CH_2OH, and (c) formic acid.

Faradaic efficiency of 33.8% with a yield rate of 17 mmol h^{-1} g_{cat}^{-1} at −0.6 V vs RHE toward acetic acid production, whereas only 21.1% maximum Faradaic efficiency with a yield rate of 59.8 mmol h^{-1} g_{cat}^{-1} at −0.8 V vs RHE was observed for formic acid (Figure 3f). Besides HCOOH and CH_3COOH, methanol (liquid product) and carbon monoxide (gaseous product) were also detected (Figures S25 and S26), whereas the obvious competing HER was not found at lower potential but was found in trace amounts at higher potentials. As the laboratory atmosphere may contain various chemicals, there is a high risk of contamination with acetic and formic acids, which can cause false-positive results. A control experiment was carried out by performing electrolysis in Ar-saturated electrolyte at −0.8 V vs RHE followed by product analysis via ^{1}H NMR spectroscopy to ensure that the observed products, i.e., HCOOH and CH_3COOH, were formed because of the electrochemical reduction of the fed CO_2 gas. The resultant ^{1}H NMR spectra (Figure S27) revealed the absence of characteristic peaks corresponding to those molecules and confirmed the successful electroreduction of CO_2 to HCOOH and CH_3COOH.

2.4. DFT Calculations

Using density functional methods akin to those employed in previous studies of porphyrin complex-catalyzed electroreduction, NO_3RR by Co-porphyrin complexes was investigated using mechanistic pathways proposed in the literature.[24,40] Collidinium/collidine and cobaltocene/cobaltocenium were used as acid−base and redox partners, respectively, to balance the studied PCET (proton-coupled electron transfer) reactions needed to reduce nitrate to ammonia and other potential products. Analysis began with the parent Co-porphyrin complex and indicated that hydrogen-bonding interactions between NO_x entities and their protonated variants were important for catalysis. The calculated free energies are given in Table S3. It is clear from the calculated energetics that the electroreduction of nitrate to ammonia is thermodynamically facile, with the majority of H^+/e^- additions being exergonic. Simulations suggest a pathway involving reduction of nitrate to nitrite/nitrous acid, which is then reduced to *NO. At this stage, H-transfer to the nitrogen of nitric acid occurs to yield nitroxyl, κ^1-O-HNO, and then *ONH_2. The former is the only H^+/e^- transfer computed to be endergonic, and only mildly so, ΔG = +1.2 kcal/mol. Addition of the next H^+/e^- is predicted to occur at the oxygen to yield a κ^1-O-hydroxylamine complex, which then undergoes a subsequent H^+/e^- addition to yield *OH and ammonia. Considering previous studies by our group,[24,40] this is hypothesized to result from the avoidance of high-energy late transition metal multiply bonded entities like *O and *N.

Analysis of several key NO_3RR intermediates suggested the presence of weak hydrogen bonds between substrate N−H and O−H bonds and the nitrogens of the porphyrin ligand. As far as determined from the computed metrics, these hydrogen bonds are weak for the parent porphyrin catalyst. More importantly, however, the DFT suggested that modification of the studied catalysts to include pendant functional groups to enhance hydrogen bonding with nitrogen-oxides and their reduced intermediates in NO_3RR would be beneficial. To evaluate this proposal, we performed the same suite of calculations on the TTPCOOH catalyst (Figures 4 and S28 and Table S3). Hydrogen bonding between the carboxyl group and various NO_3RR intermediates was significant. For example, nitric acid binding to the metal of CoTPP was computed to be mildly exergonic at −0.3 kcal/mol. However, hydrogen bonding to the COOH yielded noticeably stronger nitrate binding, −1.10 kcal/mol. Interestingly, bifunctional binding (i.e., κ^1-O + H-bonding to COOH) of nitrate was computed to be −1.6 kcal/mol for the CoTTPCOOH catalyst model; at the same level of theory, κ^1-O bonding of nitrate to

https://doi.org/10.1021/acs.chemmater.6c00705
Chem. Mater. 2026, 38, 9791−9801

Downloaded from pubs.acs.org/cmatex/article-pdf/38/19/9791/6870339/1/acs.chemmater.6c00705.pdf by UNIV OF NORTH TEXAS user on 21 October 2026

the cobalt of the parent CoTPP was mildly endergonic, ΔG_{bind} = +0.1 kcal/mol. As such, the simulations indicate that hydrogen bonding between nitrate and key NO_3RR intermediates can facilitate the catalytic process. Finally, for the parent CoTPP catalyst model, the reduction of *NO to *HNO—the most thermodynamically challenging step—was computed to be uphill by +1.2 kcal/mol. For the TTPCOOH catalyst model, this step is now exergonic, −3.4 kcal/mol. Taken together, these calculations suggest the TTPCOOH catalyst should be more active, and that H^+/e^- transfer to the *NO intermediate is the limiting step.

Preliminary DFT calculations on CO_2RR catalysis by CoTTPCOOH intermediates point to hydrogen-bonding interactions between the COOH functional group of the β-phenyl substituent. Particularly noticeable are hydrogen bonds to the ortho-COOH group and formaldehyde, $*CH_2OH$ and formic acid (Figure 5). More research is needed to further quantify the impact of these bifunctional metal—ligand interactions on the entire CO_2RR mechanism. One might expect that C_2 products to be better positioned in the active site to interact with both the metals and the β-phenyl substituents. In terms of future catalyst modifications, this research suggests profitable catalyst changes that would allow more facile bonding of the substrates to both the metal and supporting ligand functionalities on the β-substituents of the porphyrin.

3. SUMMARY AND CONCLUSIONS

In summary, the Vulcan carbon-composed cobalt tritolyl caboxy porphyrin is found to be a good bifunctional electrocatalyst for NO_3RR and CO_2RR. The CoTTPCOOH/VC achieved the highest faradic efficiency of 94.1% with NH_3 yield rate of 5.87 mmol g_{cat}^{-1} h^{-1} at −0.55 V vs RHE toward NO_3RR, whereas a maximum Faradaic efficiency of 33.8% with yield rate of 17 mmole g_{cat}^{-1} h^{-1} at −0.6 V vs RHE and 21.1% with yield rate of 59.8 mmol g_{cat}^{-1} h^{-1} at −0.8 V vs RHE were recorded for CH_3COOH and HCOOH, respectively, during CO_2RR. This material is highly stable during long-term electrolysis, without altering its physical and chemical properties. The DFT calculations also confirmed the facile binding of nitrate ions to the CoTTPCOOH. Thus, CoTTPCOOH/VC can be a powerful electrocatalyst material not only for the environmental remediation of nitrate ions and carbon dioxide gas, but also for the circular economy. Furthermore, the bifunctional activity of such materials motivates us to explore their application to the synthesis of other high-demand chemicals, such as urea, methylamine, and ethylamine, via coelectroreduction of nitrate and carbon dioxide.

4. EXPERIMENTAL METHODS

4.1. Synthesis of the Materials

4.1.1. Tritolylester Porphyrin, (1). Tritolylester porphyrin free base was synthesized by refluxing p-tolualdehyde, pyrrole, and methyl 4-formylbenzoate in propionic acid. First, 231 mL of propionic acid was poured into a 500 mL round-bottom (RB) flask and warmed for a few minutes; then p-tolualdehyde (4.91 mL, 41.61 mmol), methyl 4-formylbenzoate (2.28 g, 13.88 mmol), and pyrrole (3.85 mL, 55.45 mmol) were added and allowed to reflux for 4.5 h. Reaction progress was monitored by thin-layer chromatography (TLC) to confirm consumption of the starting materials. After completion of the reaction, the product was stored in the refrigerator for a few hours, then filtered and washed thoroughly with MeOH and water. The compound was further purified using silica gel column chromatography with a hexane: chloroform (3:7) solvent system.

4.1.2. Synthesis of Cobalt(II)-Tritolylester Porphyrin, (2). To synthesize Cobalt(II)-tritolylester porphyrin, compound 1 (0.2 g, 0.2798 mmol), cobalt acetate dihydrate (0.431 g, 2.798 mmol), and 15 mL of dry DMF were added to a 100 mL round-bottom flask under inert conditions and refluxed for 50 min to get the metalated compound. Then the solvent was removed under reduced pressure, and the product was purified by column chromatography on silica using a hexane:chloroform (4:6) solvent system.

4.1.3. Synthesis of Cobalt(II)-Tritolylcarboxy Porphyrin, (3). Compound 2 (0.1 g, 0.13 mmol), was treated with a strongly alkaline catalytic system (i.e., a mixture of 25 mL of 2 M KOH with 25 mL of ethanol) in a 100 mL round-bottom flask.[2] The whole contents were refluxed for 4—5 h and allowed to cool to room temperature; then HCl (1 M) solution was added slowly to obtain neutral pH. Thereafter, the compound was filtered, washed with water, and dried in a vacuum oven.

4.1.4. Synthesis of Tetratolylporphyrin, (4). p-tolualdehyde (2.00 g, 0.0166 mmol) and pyrrole (1.15 mL, 0.0166 mmol) were added to a 250 mL round-bottom flask containing warm propionic acid (70 mL) and allowed to reflux for 4.5 h until the completion of the reaction (observed by TLC). The mixture was kept in the refrigerator overnight, then washed with water and methanol, and finally purified by column chromatography using a hexane:chloroform (4:6) solvent system.

4.1.5. Synthesis of Cobalt-(II) Tetratolyl Porphyrin, (5). Compound 4 (0.1 g, 0.15 mmol) and cobalt acetate dihydrate (0.23 g, 1.5 mmol) were placed in a 100 mL round-bottom flask, then dry DMF (15 mL) was added under an inert atmosphere, and the reaction was refluxed for 50 min to incorporate the cobalt within the porphyrin cage. Reaction progress was monitored by UV—vis spectroscopy and TLC, and excess solvent was removed under reduced pressure. In the workup, the compound was extracted with chloroform and water, then purified by column chromatography on silica using hexane:chloroform (5:5) as the solvent system.

4.2. Characterization of the Materials

The physical and chemical characterization of the materials was conducted using various spectroscopic techniques. The electronic absorption spectra were recorded using a Shimadzu UV-2600 spectrophotometer with a pair of quartz cells (3.5 mL volume and 1 cm path length), whereas the Raman spectra were recorded using an Enwave Optronics Pro-Raman spectrometer with a 532 nm laser. Similarly, NMR, IR, and mass spectra were recorded using a Varian 500/400 MHz spectrometer and a Bruker Invenio R FTIR/PMA spectrometer, respectively. Powder X-ray diffraction (PXRD) analysis was performed using a Rigaku Smart Lab SE diffractometer with a Cu Kα source (λ = 1.5406 Å) between 3° and 80° at a scan speed of 4° min^{-1}. Physical Electronics Versaprobe II Scanning X-ray Photoelectron Spectrometer (XPS) was employed for XPS studies, and the resulting data were analyzed by CasaXPS software. The morphological attributes of the materials were analyzed using scanning electron microscopy (SEM; JEOL JSM-6610LV).

4.3. Electrochemical Studies

An EG&G 263A electrochemical analyzer, operated with PowerSuite software, was used to conduct electrochemical studies. A three-electrode setup comprising a catalyst-material-coated glassy carbon working electrode (WE), a platinum wire counter electrode (CE), and an Ag/AgCl reference electrode (RE) was assembled in a two-compartment H-cell separated by a Nafion membrane. All potential values were reported in RHE using the following conversion equation.

$$E_{RHE} = E_{Ag/AgCl} + E^0_{Ag/AgCl} + 0.059\ pH$$

4.4. Quantification of Electrolysis Products

After chronoamperometry, the electrolysis products formed in the cathodic chamber were collected and quantified using various spectroscopic techniques. UV—vis spectroscopic technique was

Downloaded from pubs.acs.org/cmatex/article-pdf/38/19/9791/6870339/1/acs.chemmater.6c00705.pdf by UNIV OF NORTH TEXAS user on 21 October 2026

https://doi.org/10.1021/acs.chemmater.6c00705
Chem. Mater. 2026, 38, 9791—9801

employed to assess ammonia, nitrite, hydrazine, and hydroxylamine via the indophenol blue method, the sulphanilamide diazotized N-(1-Naphthyl)-ethylenediamine dihydrochloride (NEDA) coupling method, the Watt and Crisp method, and the o-phenanthroline method, respectively (see SI for details of product analysis). The ^{1}H NMR spectra were recorded to analyze liquid products from CO_2RR and isotope-labeling experiments using a Varian 500 MHz spectrometer.

4.5. Computational Methodology

The Gaussian 16 code was used to compute putative intermediates in the electrocatalyzed CO_2RR and NO_3RR mechanisms. The ωB97xD functional, in conjunction with the def2-svp basis, defined the level of theory employed. Solvent effects for water were modeled using the SMD continuum model. For each stationary point, low-, medium-, and high-spin configurations were evaluated, and multiple starting geometries were analyzed to identify the lowest energy conformations. Computed free energies assumed 1 atm and 298.15 K, and the necessary thermodynamic and entropic corrections utilized unscaled vibrational frequencies.

■ ASSOCIATED CONTENT

Supporting Information

The Supporting Information is available free of charge at https://pubs.acs.org/doi/10.1021/acs.chemmater.6c00705.

Experimental details, calculation procedure, UV−vis, NMR, Raman spectra, chronoamperometric study data, UV−visible absorbance spectra for product analysis, gas chromatograms, postelectrolysis characterization evidence (PDF)

■ AUTHOR INFORMATION

Corresponding Authors

Thomas R. Cundari − *Department of Chemistry, University of North Texas, Denton, Texas 76203-5017, United States;* orcid.org/0000-0003-1822-6473; Email: Cundari@unt.edu

Francis D'Souza − *Department of Chemistry, University of North Texas, Denton, Texas 76203-5017, United States;* orcid.org/0000-0003-3815-8949; Email: Dsouza@unt.edu

Authors

Kamal Dhakal − *Department of Chemistry, University of North Texas, Denton, Texas 76203-5017, United States*

Alankar Kafle − *Department of Chemistry, University of North Texas, Denton, Texas 76203-5017, United States;* orcid.org/0009-0001-7880-7811

Swatej Sabbarwal − *Department of Chemistry, University of North Texas, Denton, Texas 76203-5017, United States*

Dili R. Subedi − *Department of Chemistry, University of North Texas, Denton, Texas 76203-5017, United States; Department of Natural Sciences, Hesston College, Hesston, Kansas 67062, United States;* orcid.org/0000-0002-5501-0201

Mohammad K. Altafi − *Department of Chemistry, University of North Texas, Denton, Texas 76203-5017, United States*

Alireza Hajiseyedjavadi − *Department of Chemistry, University of North Texas, Denton, Texas 76203-5017, United States*

Sayan Maiti − *Department of Chemistry, University of North Texas, Denton, Texas 76203-5017, United States*

Shengqian Ma − *Department of Chemistry, University of North Texas, Denton, Texas 76203-5017, United States;* orcid.org/0000-0002-1897-7069

Complete contact information is available at: https://pubs.acs.org/10.1021/acs.chemmater.6c00705

Author Contributions

[§]K.D. and A.K. contributed equally to this work. The manuscript was written with contributions from all authors. All authors have approved the final version of the manuscript. These authors contributed equally.

Notes

The authors declare no competing financial interest.

■ ACKNOWLEDGMENTS

This work was supported by the Robert A. Welch Foundation (B-2136-20260402 to T.C. and F.D.). We also gratefully acknowledge additional NSF support for the UNT CASCaM HPC cluster via grants CHE-1531468 and OAC-2117247.

■ REFERENCES

(1) Galvani, A. P.; Bauch, C. T.; Anand, M.; Singer, B. H.; Levin, S. A. Human−Environment Interactions in Population and Ecosystem Health. *Proc. Natl. Acad. Sci. U.S.A.* **2016**, *113* (51), 14502−14506.

(2) Strokal, M.; Bai, Z.; Franssen, W.; Hofstra, N.; Koelmans, A. A.; Ludwig, F.; Ma, L.; van Puijenbroek, P.; Spanier, J. E.; Vermeulen, L. C.; et al. Urbanization: An Increasing Source of Multiple Pollutants to Rivers in the 21st Century. *npj Urban Sustainability* **2021**, *1* (1), No. 24.

(3) Holdren, J. P.; Ehrlich, P. R. Human Population and the Global Environment: Population Growth, Rising Per Capita Material Consumption, and Disruptive Technologies Have Made Civilization a Global Ecological Force. *Am. Sci.* **1974**, *62* (3), 282−292.

(4) Samanta, R.; Manna, B. K.; Trivedi, R.; Chakraborty, B.; Barman, S. Hydrogen Spillover Enhances Alkaline Hydrogen Electrocatalysis on Interface-Rich Metallic Pt-Supported MoO_3. *Chem. Sci.* **2023**, *15* (1), 364−378.

(5) Manna, B. K.; Samanta, R.; Trivedi, R. K.; Chakraborty, B.; Barman, S. Hydrogen Spillover Inspired Bifunctional Platinum/Rhodium Oxide−Nitrogen-Doped Carbon Composite for Enhanced Hydrogen Evolution and Oxidation Reactions in Base. *J. Colloid Interface Sci.* **2024**, *670*, 258−271.

(6) Sharifian, R.; Wagterveld, R.; Digdaya, I.; Xiang, C.-X.; Vermaas, D. Electrochemical Carbon Dioxide Capture to Close the Carbon Cycle. *Energy Environ. Sci.* **2021**, *14* (2), 781−814.

(7) Abascal, E.; Gómez-Coma, L.; Ortiz, I.; Ortiz, A. Global Diagnosis of Nitrate Pollution in Groundwater and Review of Removal Technologies. *Sci. Total Environ.* **2022**, *810*, No. 152233.

(8) Nunes, L. J. R. The Rising Threat of Atmospheric CO_2: A Review on the Causes, Impacts, and Mitigation Strategies. *Environments* **2023**, *10* (4), No. 66.

(9) Singh, S.; Anil, A. G.; Kumar, V.; Kapoor, D.; Subramanian, S.; Singh, J.; Ramamurthy, P. C. Nitrates in the Environment: A Critical Review of Their Distribution, Sensing Techniques, Ecological Effects and Remediation. *Chemosphere* **2022**, *287*, No. 131996.

(10) Saravanan, A.; Kumar, P. S.; Vo, D.-V. N.; Jeevanantham, S.; Bhuvaneswari, V.; Narayanan, V. A.; Yaashikaa, P.; Swetha, S.; Reshma, B. A Comprehensive Review on Different Approaches for CO_2 Utilization and Conversion Pathways. *Chem. Eng. Sci.* **2021**, *236*, No. 116515.

(11) Navaee, A.; Salimi, A. Review on CO_2 Management: From CO_2 Sources, Capture, and Conversion to Future Perspectives of Gas-Phase Electrochemical Conversion and Utilization. *Energy Fuels* **2024**, *38* (4), 2708−2742.

(12) Richa, A.; Touil, S.; Fizir, M. Recent Advances in the Source Identification and Remediation Techniques of Nitrate-Contaminated Groundwater: A Review. *J. Environ. Manage.* **2022**, *316*, No. 115265.

Downloaded from pubs.acs.org/cmatex/article-pdf/38/19/9791/6870339/1/acs.chemmater.6c00705.pdf by UNIV OF NORTH TEXAS user on 21 October 2026

(13) Choudhary, M.; Muduli, M.; Ray, S. A Comprehensive Review on Nitrate Pollution and Its Remediation: Conventional and Recent Approaches. *Sustainable Water Resour. Manage.* **2022**, *8* (4), No. 113.
(14) Zeng, Y.; Priest, C.; Wang, G.; Wu, G. Restoring the Nitrogen Cycle by Electrochemical Reduction of Nitrate: Progress and Prospects. *Small Methods* **2020**, *4* (12), No. 2000672.
(15) Kempasiddaiah, M.; Samanta, R.; Panigrahy, S.; Trivedi, R. K.; Chakraborty, B.; Barman, S. Electrochemical Reconstruction of a 1D Cu(PyDC)(H_2O) MOF into *in situ* Formed Cu−Cu_2O Heterostructures on Carbon Cloth as an Efficient Electrocatalyst for CO_2 Conversion. *Nanoscale* **2024**, *16* (21), 10458−10473.
(16) Samanta, R.; Kempasiddaiah, M.; Trivedi, R. K.; Chakraborty, B.; Barman, S. Sn/SnO_2 Nanocomposite Encapsulated on Nitrogen-Doped Carbon as a Highly Efficient Catalyst for the Electrochemical Reduction of CO_2 to Formate. *ACS Appl. Energy Mater.* **2024**, *7* (13), 5359−5370.
(17) Kempasiddaiah, M.; Samanta, R.; Trivedi, R. K.; Shrivastava, D.; Chakraborty, B.; Barman, S. Single-Crystalline α-Bi_2O_3 Induced by Nitrogen Doping for Enhanced and Selective CO_2 Electroreduction to Formate over a Wide Negative Potential Window. *ACS Appl. Energy Mater.* **2024**, *7* (19), 8465−8477.
(18) Wang, Z.; Young, S. D.; Goldsmith, B. R.; Singh, N. Increasing Electrocatalytic Nitrate Reduction Activity by Controlling Adsorption through PtRu Alloying. *J. Catal.* **2021**, *395*, 143−154.
(19) Chen, Y.; Zohaib, A.; Sun, H.; Sun, S. Multi-Metallic Nanoparticles: Synthesis and Their Catalytic Applications. *Chem. Commun.* **2025**, *61* (65), 12097−12114.
(20) Kaur, S.; Garg, K.; Gupta, D.; Kafle, A.; Dharmender; Shukla, V.; Ahuja, R.; Nagaiah, T. C. Unleashing High-Yield Urea Production by Pulse Electrodeposition of Bi/Cu via Co-Reduction of N_2 and CO_2. *ACS Energy Lett.* **2025**, *10* (1), 85−93.
(21) Guragain, M.; Kafle, A.; Adesope, Q.; Altafi, M. K.; Amagbor, S. C.; Mesilov, V.; Kelber, J. A.; Cundari, T. R.; D'Souza, F. Photoenhanced Electrochemical Conversion of Nitrate to Ammonia via Sulfur Vacancy-Rich Exfoliated MoS_2. *ACS Catal.* **2024**, *14* (23), 18085−18094.
(22) Kularathne, P. P.; Kafle, A.; Gharaee, M.; Mudiyanselage, R. N.; Guragain, M.; Adesope, Q.; Kelber, J. A.; Cundari, T. R.; D'Souza, F. Selective Ammonia Synthesis via Electrocatalytic Nitrate Reduction Reaction on Molybdenum Selenide with Selenium Vacancy. *Energy Fuels* **2025**, *39* (36), 17543−17551.
(23) Liu, Y.; Huang, C. Recent Advances in Metal Chalcogenide Catalysts for Electrochemical Carbon Dioxide Reduction. *Adv. Funct. Mater.* **2025**, *35*, No. 2505245.
(24) Duan, X.; Xu, J.; Wei, Z.; Ma, J.; Guo, S.; Wang, S.; Liu, H.; Dou, S. Metal-Free Carbon Materials for CO_2 Electrochemical Reduction. *Adv. Mater.* **2017**, *29* (41), No. 1701784.
(25) Liao, G.; Smith, R. L., Jr.; Guo, H.; Qi, X. Review of Carbon-Based Catalysts for Electrochemical Nitrate Reduction and Green Ammonia Synthesis. *Green Chem.* **2024**, *26* (24), 11797−11831.
(26) Liu, X.; Liu, X.-H.; Zhang, X.; Wang, H.; Zhao, Q. Metal−Organic Frameworks and Their Derivatives for the Electrochemical CO_2 Reduction Reaction: Insights from Molecular Engineering. *J. Mater. Chem. A* **2024**, *12* (32), 20578−20605.
(27) Nam, D.-H.; Shekhah, O.; Lee, G.; Mallick, A.; Jiang, H.; Li, F.; Chen, B.; Wicks, J.; Eddaoudi, M.; Sargent, E. H. Intermediate Binding Control Using Metal−Organic Frameworks Enhances Electrochemical CO_2 Reduction. *J. Am. Chem. Soc.* **2020**, *142* (51), 21513−21521.
(28) Fang, J.; Zhu, Y.-N.; Long, X.; Li, X.-B.; Zhang, Q.; Yang, G.; Du, S.; Liu, Z.; Liu, Z.; Peng, F. Theoretical Calculations and Experimental Verification of Carbon Dioxide Reduction Electrocatalyzed by Metalloporphyrin. *J. Colloid Interface Sci.* **2024**, *668*, 366−374.
(29) Dhakal, K.; Subedi, D. R.; Hajiseyedjavadi, A.; Guragain, M.; Kafle, A.; Kelber, J. A.; Cundari, T. R.; D'Souza, F. Porphyrin-Based Conductive Polymer Derived from Tetrakis[biphenyl-bis-(bithiophene)] Porphyrinato Cobalt(II) for Efficient Electrochemical Nitrate Reduction to Ammonia. *ChemSusChem* **2025**, *18*, No. e202500183.
(30) Harmon, N. J.; Li, J.; Wang, B. T.; Gao, Y.; Wang, H. Influence of Carbon Nanotube Support on Electrochemical Nitrate Reduction Catalyzed by Cobalt Phthalocyanine Molecules. *ACS Catal.* **2024**, *14* (5), 3575−3581.
(31) Wang, M.; Torbensen, K.; Salvatore, D.; Ren, S.; Joulié, D.; Dumoulin, F.; Mendoza, D.; Lassalle-Kaiser, B.; Işci, U.; Berlinguette, C. P.; Robert, M. CO_2 Electrochemical Catalytic Reduction with a Highly Active Cobalt Phthalocyanine. *Nat. Commun.* **2019**, *10* (1), No. 3602.
(32) Ren, S.; Joulié, D.; Salvatore, D.; Torbensen, K.; Wang, M.; Robert, M.; Berlinguette, C. P. Molecular Electrocatalysts Can Mediate Fast, Selective CO_2 Reduction in a Flow Cell. *Science* **2019**, *365* (6451), 367−369.
(33) Sun, L.; Reddu, V.; Fisher, A. C.; Wang, X. Electrocatalytic Reduction of Carbon Dioxide: Opportunities with Heterogeneous Molecular Catalysts. *Energy Environ. Sci.* **2020**, *13* (2), 374−403.
(34) Wang, H.; Ma, C.; Lu, Q.; Gu, M.; Jiang, L.; Hao, Y.; Hu, F.; Li, L.; Wang, G.; Peng, S. Precise Tuning of Functional Group Spatial Distribution on Porphyrin Rings for Enhanced CO_2 Electroreduction Selectivity. *Angew. Chem., Int. Ed.* **2025**, *64* (19), No. e202501091.
(35) Elgrishi, N.; Griveau, S.; Chambers, M. B.; Bedioui, F.; Fontecave, M. Versatile Functionalization of Carbon Electrodes with a Polypyridine Ligand: Metallation and Electrocatalytic H+ and CO_2 Reduction. *Chem. Commun.* **2015**, *51* (14), 2995−2998.
(36) Lu, Y.; Li, W.; Fan, Y.; Cheng, L.; Tang, Y.; Sun, H. Recent Advances in Bonding Regulation of Metalloporphyrin-Modified Carbon-Based Catalysts for Accelerating Energy Electrocatalytic Applications. *Small* **2024**, *20* (51), No. 2406180.
(37) Jiang, H.; Zhao, P.; Shen, H.; Yang, S.; Gao, R.; Guo, Y.; Cao, Y.; Zhang, Q.; Zhang, H. New Insight into the Electronic Effect for Cu Porphyrin Catalysts in Electrocatalytic Conversion of CO_2 into CH_4. *Small* **2024**, *20* (2), No. 2304998.
(38) Sun, H.; Zhang, W.; Qi, Y.; Xu, Q.; Han, J.; Wu, J.; Qin, J. S.; Rao, H. Cation-Engineered Iron Porphyrin Boosting Electrocatalytic Reduction of Nitrite to Ammonia. *Angew. Chem., Int. Ed.* **2025**, *64* (48), No. e202513890.
(39) Maurin, A.; Robert, M. Catalytic CO_2-to-CO Conversion in Water by Covalently Functionalized Carbon Nanotubes with a Molecular Iron Catalyst. *Chem. Commun.* **2016**, *52* (81), 12084−12087.
(40) Choi, J.; Wagner, P.; Jalili, R.; Kim, J.; MacFarlane, D. R.; Wallace, G. G.; Officer, D. L. A Porphyrin/Graphene Framework: A Highly Efficient and Robust Electrocatalyst for Carbon Dioxide Reduction. *Adv. Energy Mater.* **2018**, *8* (26), No. 1801280.
(41) Anton, J. A.; Loach, P. A. Synthesis of Some Mono-, Di-, and Trisubstituted Tetraarylporphyrins. *J. Heterocycl. Chem.* **1975**, *12* (3), 573−576.
(42) Parthasarathi, N.; Hansen, C.; Yamaguchi, S.; Spiro, T. Metalloporphyrin Core Size Resonance Raman Marker Bands Revisited: Implications for the Interpretation of Hemoglobin Photoproduct Raman Frequencies. *J. Am. Chem. Soc.* **1987**, *109* (13), 3865−3871.
(43) Roy, D. R.; Shah, E. V.; Roy, S. M. Optical Activity of Co-Porphyrin in the Light of IR and Raman Spectroscopy: A Critical DFT Investigation. *Spectrochim. Acta, Part A* **2018**, *190*, 121−128.
(44) Tutunea, F.; Ryan, M. D. Visible and Infrared Spectroelectrochemistry of Cobalt Porphinones and Porphinediones. *J. Electroanal. Chem.* **2012**, *670*, 16−22.
(45) Sonkar, P. K.; Prakash, K.; Yadav, M.; Ganesan, V.; Sankar, M.; Gupta, R.; Yadav, D. K. Co(II)-Porphyrin-Decorated Carbon Nanotubes as Catalysts for Oxygen Reduction Reactions: An Approach for Fuel Cell Improvement. *J. Mater. Chem. A* **2017**, *5* (13), 6263−6276.
(46) Thakur, P. S.; Singh, V.; Ganesan, V.; Sankar, M. Porphyrin-Based Covalent Organic Framework Encapsulating Multiwalled Carbon Nanotubes: A High-Performance Electrocatalyst for Oxygen Reduction Reaction. *Langmuir* **2025**, *41* (16), 10456−10468.

Downloaded from pubs.acs.org/cmatex/article-pdf/38/19/9791/6870339l/acs.chemmater.6c00705.pdf by UNIV OF NORTH TEXAS user on 21 October 2026

https://doi.org/10.1021/acs.chemmater.6c00705
Chem. Mater. 2026, 38, 9791−9801

(47) Manhas, S.; Khajuria, S.; Verma, M.; Ahmed, S.; Bhat, A. R.; Upadhye, V. J.; Kundan, S. Graphene Oxide Functionalized Metalloporphyrins as Advanced Antimicrobial Nanomaterials with Integrated Synthesis, Characterization and Molecular Docking Evaluations. *Sci. Rep.* **2026**, *16*, No. 3455.
(48) Wu, Z.-Y.; Chen, M.-X.; Chu, S.-Q.; Lin, Y.; Liang, H.-W.; Zhang, J.; Yu, S.-H. Switching Co/N/C Catalysts for Heterogeneous Catalysis and Electrocatalysis by Controllable Pyrolysis of Cobalt Porphyrin. *iScience* **2019**, *15*, 282−290.
(49) Zhutaeva, G. V.; Bogdanovskaya, V. A.; Davydova, E. S.; Kazanskii, L. P.; Tarasevich, M. R. Kinetics and Mechanism of Oxygen Electroreduction on Vulcan XC72R Carbon Black Modified by Pyrolysis Products of Cobalt 5,10,15,20-Tetrakis(4-methoxyphenyl)porphyrin in a Broad pH Interval. *J. Solid State Electrochem.* **2014**, *18* (5), 1319−1334.
(50) Orellana, W.; Loyola, C. Z.; Marco, J. F.; Tasca, F. Evidence of Carbon-Supported Porphyrins Pyrolyzed for the Oxygen Reduction Reaction Keeping Integrity. *Sci. Rep.* **2022**, *12* (1), No. 8072.
(51) Wei, Y.; Liang, Y.; Wu, Q.; Xue, Z.; Feng, L.; Zhang, J.; Zhao, L. Effects of Tuning the Structural Symmetry of Cobalt Porphyrin on Electrocatalytic Oxygen Reduction Reactions. *Dalton Trans.* **2023**, *52* (40), 14573−14582.
(52) Jiang, L.; Cui, L.; He, X. Cobalt-Porphyrin Noncovalently Functionalized Graphene as Nonprecious-Metal Electrocatalyst for Oxygen Reduction Reaction in an Alkaline Medium. *J. Solid State Electrochem.* **2015**, *19* (2), 497−506.
(53) Choi, J.; Kim, J.; Wagner, P.; Gambhir, S.; Jalili, R.; Byun, S.; Sayyar, S.; Lee, Y. M.; MacFarlane, D. R.; Wallace, G. G.; Officer, D. L. Energy Efficient Electrochemical Reduction of CO_2 to CO Using a Three-Dimensional Porphyrin/Graphene Hydrogel. *Energy Environ. Sci.* **2019**, *12* (2), 747−755.
(54) Zhu, M.; Cao, C.; Chen, J.; Sun, Y.; Ye, R.; Xu, J.; Han, Y.-F. Electronic Tuning of Cobalt Porphyrins Immobilized on Nitrogen-Doped Graphene for CO_2 Reduction. *ACS Appl. Energy Mater.* **2019**, *2* (4), 2435−2440.
(55) Kafle, A.; Gupta, D.; Bordoloi, A.; Nagaiah, T. C. Self-Standing Fe_3O_4-Decorated Paper Electrode as Binder-Free Trifunctional Electrode for Electrochemical Ammonia Synthesis and Zn−O2 Batteries. *Nanoscale* **2022**, *14*, 16590−16601.
(56) Gupta, D.; Kafle, A.; Singh, M.; Kumar, S.; Nagaiah, T. C. Real-Time Screening of Ni_xB_y Bifunctional Electrocatalysts for Overall NH_3 Synthesis via SG-TC SECM. *Mater. Horiz.* **2024**, *11* (5), 1212−1222.

Downloaded from pubs.acs.org/cmatex/article-pdf/38/19/9791/6870339/1/acs.chemmater.6c00705.pdf by UNIV OF NORTH TEXAS user on 21 October 2026

https://doi.org/10.1021/acs.chemmater.6c00705
Chem. Mater. 2026, 38, 9791−9801